Influence of surfactant solubility on the deformation and breakup of a bubble or capillary jet in a viscous fluid

Y.-N. Young,[1] M. R. Booty,[1] M. Siegel,[1] and J. Li[2]
[1]*Department of Mathematical Sciences and Center for Applied Mathematics and Statistics, New Jersey Institute of Technology, Newark, New Jersey 07102, USA*
[2]*Department of Engineering, Cambridge University, Cambridge CB2 1PZ, United Kingdom*

(Received 30 January 2009; accepted 19 June 2009; published online 15 July 2009)

In a previous study [M. Hameed *et al.*, J. Fluid Mech. **594**, 307 (2008)] the authors investigated the influence of insoluble surfactant on the evolution of a stretched, inviscid bubble surrounded by a viscous fluid via direct numerical simulation of the Navier–Stokes equations, and showed that the presence of surfactant can cause the bubble to contract and form a quasisteady slender thread connecting parent bubbles, instead of proceeding directly toward pinch-off as occurs for a surfactant-free bubble. Insoluble surfactant significantly retards pinch-off and the thread is stabilized by a balance between internal pressure and reduced capillary pressure due to a high concentration of surfactant that develops during the initial stage of contraction. In the present study we investigate the influence of surfactant solubility on thread formation. The adsorption-desorption kinetics for solubility is in the diffusion controlled regime. A long-wave model for the evolution of a capillary jet is also studied in the Stokes flow limit, and shows dynamics that are similar to those of the evolving bubble. With soluble surfactant, depending on parameter values, a slender thread forms but can pinch-off later due to exchange of surfactant between the interface and exterior bulk flow.
 [DOI: 10.1063/1.3176462]

I. INTRODUCTION

The surface tension-driven deformation and breakup of a stretched droplet or liquid thread suspended in a viscous fluid is a significant event in many fluid processes, including emulsion formation, mixing in multiphase fluid systems, fiber coating, and ink-jet printing. Detailed understanding of the evolution and pinch-off of drops and threads is motivated by the desire to predict and control detached drop volume, or to suppress satellite drops. Recent interest in droplet breakup also stems from applications in micro- and nanofluidic technologies. For example, devices have been developed to promote instability of the interface between coflowing liquids to form uniform, micron-sized droplets or bubbles,[1–3] with potential applications in drug delivery and medical imaging. Recent reviews[4–7] summarize research on instability and breakup of droplets, threads, and coatings and include discussions of the relevant technological applications.

Much research has focused on drop and thread deformation and breakup in clean fluid systems for which interfacial tension gradients are absent. Theoretical study of the dynamics of surfactant-free liquid threads was initiated by the linear stability analyses of Rayleigh[8,9] and Tomotika,[10] while more recent investigations often utilize one-dimensional long-wave approximations to the governing equations.[11–13] These investigations have combined with experiments, numerical studies, scaling theories, and local similarity solutions to provide a relatively complete picture of the dynamics in a neighborhood of the space-time singularity at pinch-off.[14–19]

In many applications, surfactants (or surface contaminants) are used to control droplet size by lowering surface tension. Variations in surface tension that are introduced by surfactant can substantially alter interfacial evolution and flow. A striking example is the tip streaming of thin threads or small droplets from a deformed bubble in an imposed shear or strain. Although first observed by Taylor[20] in his seminal four-roller mill experiments, tip streaming has only recently been ascribed to the presence of surfactant.[21–23] Surfactant mediated tip streaming has recently been utilized to synthesize micrometer-sized and smaller droplets.[24]

Experiments and analyses[25] show that surfactant has a significant effect on the stability of a viscous jet surrounded by another viscous fluid. Linear stability analysis[26–28] of the influence of surfactant on the evolution of a cylindrical capillary jet surrounded by another viscous fluid shows that surfactant slows the growth rate of disturbances due to a combination of reduced surface tension and the immobilizing (surface stiffening) effect of the Marangoni stress. Most research of surfactant effects on the nonlinear evolution of drops and threads has been focused on the case of a viscous thread surrounded by a passive inviscid fluid or on viscosity matched liquids, in the presence of insoluble surfactant. Investigations utilizing one-dimensional long-wave approximations to the governing equations confirm that surfactant delays pinching, and together with scaling theories show that when a viscous jet approaches pinch-off, surfactant is swept away from the narrowing neck or waist due to the interior flow, and its presence has a minimal effect on the detailed dynamics near pinch-off.[25,27] Numerical studies[29–31] of the effect of insoluble surfactant on the deformation and pinch-off of jets and drops verify many of the conclusions obtained from long-wave approximations.

Different dynamics are found for an inviscid or nearly inviscid insoluble surfactant-laden jet that is surrounded by a

more viscous fluid.[32] Using direct numerical simulation and a long-wave model for an inviscid jet in the Stokes flow limit, it is found that the direction of the exterior flow during contraction of the interface due to capillary instability is nearly radial, with the result that surfactant concentration is greatly increased where a neck forms, and in the absence of surfactant, this is the location of pinch-off in finite time. In the presence of surfactant, however, breakup is impeded and a long thin thread forms. The underlying mechanism for thread formation is the reduction in surface tension due to high concentration of surfactant at the neck. The surface tension is found to decrease sufficiently rapidly relative to the decrease in neck radius that the capillary pressure approaches the pressure of the internal fluid before the neck radius tends to zero. The decrease in neck radius is interrupted when these two forces balance, before pinch-off can occur. Typically, thin thread formation occurs when surface tension is reduced by a factor of 3–10 relative to its surfactant-free value. As a result, capillary contraction halts, and a quasisteady long thin thread forms, connecting two parent bubbles. The interface eventually pinches off at constrictions that connect the thread ends to the parent bubbles. A long-wave asymptotic model for a capillary jet covered with surfactant explains the principle mechanism of slender thread formation and confirms, for example, the relatively minor role of the Marangoni stress in this process. On the other hand, the late-time evolution of the thread and its eventual breakup are dependent on the distribution of the Marangoni stress and surface diffusion of surfactant.

In micro- and nanofluidic experiments, soluble surfactants may be preferred for controlling droplet dynamics and size distribution. A new microfluidic method for production of submicrometer and potentially nanoscale droplets and particles utilizes moderate concentration of soluble surfactant in an elongational flow to create small droplets via tip streaming in a flow-focusing microfluidic device.[24] An elongational flow draws a drop of a different fluid phase at the orifice of a capillary tube and focuses its tip, stretching the interface and causing a gradient of surfactant concentration along it. Under the right conditions, surfactants are adsorbed to the interface from the bulk flow and cannot desorb fast enough compared to their rate of compression along it so that the tip becomes highly packed with surfactant. This leads to a sharp decrease in the interfacial tension and a highly curved tip.[21,33] When its surfactant concentration is sufficiently large, the highly curved tip is drawn into a thin thread, which subsequently breaks into tiny surfactant-laden droplets, leaving the interface temporarily depleted of surfactant.

The application of surfactants in microfluidic devices motivates our study of the effects of surfactant solubility on bubble and thread breakup. Previous theoretical[34,35] and computational[36–39] investigations of the effects of soluble surfactant on drop dynamics have mainly considered the rise of drops and bubbles in a quiescent fluid. Boundary integral numerical methods were employed by Milliken and Leal[40] to examine a viscous drop strained by an extensional flow, and by Johnson and Borhan[41] to investigate a buoyant translating drop. These last two studies impose the computationally tractable but less physically realizable limit $\mathrm{Pe} \ll 1$, where Pe is the bulk Peclet number that measures the ratio of bulk convective to diffusive transport. Recently, front tracking[42,43] and diffuse interface[44] numerical methods have been designed to treat the effect of soluble surfactant on translating or rising bubbles, and on drops in extensional flow.

In work more closely related to our study, Jin *et al.*[45] investigated numerically how different surfactant adsorption-desorption dynamics influence the necking process of a viscous drop that is injected from a tube into another viscous fluid. This process depends sensitively on the surface concentration of surfactant at the onset of necking, which in turn depends on the adsorption rate of surfactant as the interface expands out of the tube. Here, we consider the situation of an initially surfactant-coated, prestretched bubble evolving in an otherwise quiescent fluid. This allows us to isolate the influence of parameter values (e.g., surfactant rate constants) on necking and pinch-off from their effect on surfactant adsorption at a rapidly expanding interface, as occurs in bubble injection.

Since surfactant effects are more significant for pinch-off at low internal viscosities, we focus on the influence of surfactant solubility on the dynamics of an inviscid drop in a viscous fluid. To this end, our previous simulations and long-wave asymptotic model for insoluble surfactant[32] are extended to investigate how surfactant exchange between an interface and bulk affects the dynamics. Our investigations include numerical simulations of the Navier–Stokes equations for a slender inviscid bubble evolving in a viscous exterior fluid in the presence of both surface and bulk surfactant concentrations. We also derive a long-wave model for an inviscid capillary jet with surfactant exchange. Results of the long-wave model provide insight into the formation and shape of quasisteady threads that are observed in the numerical simulations of a collapsing bubble, and allow us to gauge the relative magnitude of different physical effects that occur during the evolution.

Details of the initial prestretched, dumbbell bubble profile and other initial conditions for this study are described in Sec. III, but we note here that the bulk and surface surfactant concentrations are not in equilibrium at the initial instant. Since the diffusion coefficient D of surfactants[46] is of the order of 10^{-10} $\mathrm{m}^2\,\mathrm{s}^{-1}$, for a spherical bubble, from which the dumbbell profile is formed, a radius as small as $a=0.1$ mm implies a time scale for diffusion of surfactant in the bulk phase of the order of $a^2/D \simeq 10^2$ s, which is much greater than the duration of the prestretching phase. As a consequence, while the surface concentration of surfactant is reduced by the increase in interfacial area during the prestretching phase, diffusion of surfactant in the bulk does not have sufficient time to restore surfactant concentrations in the two different phases to equilibrium. The influence of bulk surfactant diffusion alone immediately after the initial instant is therefore to increase the surface surfactant concentration.

The paper is organized as follows. The problem formulation and governing equations are given in Sec. II, which includes a brief description of development of the numerical method to include the treatment of bulk surfactant concentration and bulk-interface coupling. In Sec. III results of direct numerical simulations with low Reynolds number

(Re≃0.25) and various values of the surfactant rate coefficients and bulk Peclet number are presented to illustrate the effects of surfactant solubility on thread formation during the capillary contraction of a bubble. Surfactant exchange between the bulk and interface leads to different thread dynamics, including different locations for bubble pinch-off. In Sec. IV a long-wave model is derived for the evolution of a capillary jet with soluble surfactant in the Stokes flow limit and results of its numerical solution are presented. Concluding remarks are given in Sec. V.

II. PROBLEM FORMULATION

The flow in the exterior fluid is governed by the incompressible Navier–Stokes equations

$$\mathrm{Re}(\partial_t + \boldsymbol{u}\cdot\nabla)\boldsymbol{u} = -\nabla p + \nabla^2\boldsymbol{u}, \tag{1}$$

$$\nabla\cdot\boldsymbol{u} = 0, \tag{2}$$

for a fluid with constant viscosity μ and constant density ρ. Lengths are nondimensionalized by the radius a of an undeformed spherical bubble of the same volume, and the velocity $\boldsymbol{u}$ is made nondimensional by the surface tension-driven value $U=\sigma^*/\mu$, where σ^* is the surface tension of a "clean" or surfactant-free bubble. Time is made nondimensional by a/U, while the pressure inside the bubble p_i and outside the bubble p are made nondimensional by $\mu U/a$. The Reynolds number is $\mathrm{Re}=Ua/\nu$ where ν is the kinematic viscosity of the exterior fluid.

When the interior fluid is inviscid, the pressure inside the bubble $p_i=p_i(t)$ is a function of time alone, and incompressibility of the interior fluid implies that the bubble volume is conserved, i.e.,

$$V = \tfrac{4}{3}\pi. \tag{3}$$

For an inviscid bubble, this must be imposed as a condition that is required to find $p_i(t)$.

The bubble surface S has equation $F(\boldsymbol{x},t)=0$, and the kinematic boundary condition is

$$\frac{d\boldsymbol{x}}{dt} = (\boldsymbol{u}\cdot\boldsymbol{n})\boldsymbol{n} \tag{4}$$

for the motion of a point on the interface $\boldsymbol{x}$ in the normal direction $\boldsymbol{n}$, which was chosen to point outward from S. The continuity of stress boundary condition on S takes the form

$$(p_i - p)\boldsymbol{n} + 2\boldsymbol{e}\cdot\boldsymbol{n} = \sigma(\kappa_\theta + \kappa_z)\boldsymbol{n} - \nabla_s\sigma, \tag{5}$$

where $\boldsymbol{e}$ is the rate of strain tensor, κ_θ and κ_z are the principal normal curvatures of S, the surface tension σ has been made nondimensional by σ^*, and ∇_s is the surface gradient $\nabla_s=\nabla-\boldsymbol{n}(\boldsymbol{n}\cdot\nabla)$.

The bulk concentration of soluble surfactant C is made nondimensional by the value at infinity C_∞, while the concentration of surfactant adsorbed on the bubble surface Γ is made nondimensional by the value of the maximum concentration for monolayer adsorption Γ_∞. In the diffusion controlled regime, the equations for evolution of adsorbed and bulk surfactant are

$$\frac{\partial\Gamma}{\partial t} + \nabla_s\cdot(\boldsymbol{u}_s\Gamma) + (\kappa_\theta+\kappa_z)\Gamma\boldsymbol{u}\cdot\boldsymbol{n} = \frac{1}{\mathrm{Pe}_s}\nabla_s^2\Gamma + J\boldsymbol{n}\cdot\nabla C|_s, \tag{6}$$

$$\frac{\partial C}{\partial t} + \boldsymbol{u}\cdot\nabla C = \frac{1}{\mathrm{Pe}}\nabla^2 C. \tag{7}$$

Here, $\boldsymbol{u}_s$ is the tangential fluid velocity on S, $\mathrm{Pe}_s=Ua/D_s$ is the Peclet number for surface diffusion of adsorbed surfactant, and $\mathrm{Pe}=Ua/D$ is the Peclet number for bulk diffusion of surfactant, where D_s and D are the respective surface and bulk diffusivities. The last term on the right-hand side of Eq. (6) represents the transfer or exchange of surfactant between its bulk form in the suspending fluid and its adsorbed form in the monolayer on the bubble surface due to diffusive flux of surfactant immediately outside S, and the parameter $J=C_\infty D/\Gamma_\infty U$ is a measure of the efficiency of this process.

In Eq. (6) the net transport of surfactant onto S is given by a Fickian diffusive flux, while the rates of adsorption and desorption between S and the neighboring fluid are assumed to be sufficiently fast to be in mutual equilibrium. When the Langmuir isotherm is used to model the adsorption-desorption kinetics, this leads to a relation between the bulk surfactant concentration immediately adjacent to the bubble surface $C|_s$ and the surface concentration Γ, given by[41]

$$C|_s = \frac{\Gamma}{K(1-\Gamma)}. \tag{8}$$

Here, $K=\kappa_1 C_\infty/\kappa_2$ is a dimensionless equilibrium partition coefficient, representing the ratio of the characteristic adsorption rate κ_1 to the desorption rate κ_2 at the interface. The boundary condition

$$C \to 1 \quad \text{as} \quad |\boldsymbol{x}| \to \infty \tag{9}$$

is implied by the nondimensionalization of C.

A widely used nonlinear equation of state, relating the surface tension σ to the adsorbed surfactant concentration Γ, is the Langmuir equation $\sigma=1+E\ln(1-\Gamma)$, where the elasticity number $E=RT\Gamma_\infty/\sigma^*$ is a measure of the sensitivity of surface tension to changes in the concentration of adsorbed surfactant on S. During thread formation, sufficiently high surfactant concentrations can develop that the Langmuir equation ceases to be a good fit to experimental data at values of Γ beyond which the integrity of the surfactant monolayer is compromised by micelle formation. As in Refs. 32 and 42, we adopt a modified Langmuir equation of state, given by

$$\sigma = \max(1 + E\ln(1-\Gamma), \sigma_{\min}). \tag{10}$$

This prescribes a minimum surface tension $\sigma_{\min}$ without maintaining exact conservation of surfactant in the separate monolayer, dissolved and micelle phases when the bulk surfactant concentration is at the critical micelle concentration (CMC). Values of $\sigma_{\min}$ vary for different fluid-surfactant systems. Here, the minimum saturated value of the surface tension is taken to be $\sigma_{\min}=0.1$, and this value was reported under equilibrium conditions by, for example, DeBruijn.[22] In this study, the minimum surface tension is encountered only

once, in solution of the long-wave model equations at large Pe in Sec. IV B.

The case of an insoluble surfactant is recovered in the limit $J \to 0$, in which there is no transfer of surfactant between the bulk and surface phases, and Eq. (7) and boundary condition (8) become uncoupled. The parameters J, K, and Pe are not independent and are related by

$$J = \frac{\chi K}{\mathrm{Pe}}, \quad \text{where } \chi = \frac{\kappa_2 a}{\kappa_1 \Gamma_\infty}. \tag{11}$$

A. Numerical method

The numerical method uses an arbitrary Lagrangian–Eulerian (ALE) moving mesh with a body-fitted grid, in which the interface is a line of the grid, and dynamic boundary conditions at the interface are incorporated accurately within a finite-volume formulation. ALE methods were first developed in the context of finite-difference and finite-volume methods, and a recent review was given by Donea and Huerta.[47] ALE methods with finite elements and novel meshing strategies have also been applied to studies of drop breakup.[14,48,49]

The method used here is based on one developed for insoluble surfactant by Li *et al.*[50] and Li,[51] and was used in our earlier study on the influence of insoluble surfactant on the breakup of an inviscid bubble or jet.[32] For use with soluble surfactant, Eq. (6) for the surface concentration Γ is solved by modifying the same fractional step, finite-volume method [see Eqs. (2.9)–(2.12) in Ref. 32]. This places the discretization $\mathcal{J}^n_{i+1/2}$ of the term $J\boldsymbol{n}\cdot\nabla C|_S$ for transfer of surfactant between the interface and the bulk in the first part of the time step, together with the discretizations for the surface advective and diffusive fluxes of Γ, to evaluate $\Gamma^{n+1/2}_{i+1/2}$. The bulk concentration C and its normal derivative are discretized at the center of a computational cell, in the same way as, for example, the pressure. The normal derivative is weighted by the area element $\Delta S^n_{i+1/2}$ for computing the interface-bulk exchange flux. In the second part of the time step, Γ is updated by the change in the area element due to the interface normal velocity; the total amount of surfactant within an area element is conserved, and the concentration $\Gamma^{n+1}_{i+1/2}$ is found by computing the updated area element $\Delta S^{n+1}_{i+1/2}$ when the interface mesh markers $\boldsymbol{r}^n_i$ are updated to $\boldsymbol{r}^{n+1}_i$. In the limit $J=0$ of insoluble surfactant, this conserves the total amount of surfactant on S at each time step up to round-off error.

In Eq. (7) for the evolution of C, first order forward differencing is used for the time derivative and, away from S, $C^{n+1}_{i+1/2,j+1/2}$ is evaluated at the center of each computational cell by a second order weighted finite-difference scheme for the advective and diffusive flux terms, in much the same way as the velocity is updated at the corner of each cell in the momentum equation. Adjacent to $S(j=1)$ the advective flux is evaluated by the same upwinding scheme[32,51] as is used in Eq. (6) for Γ, while on S, $C^{n+1}_{i+1/2,0}$ is computed from Eq. (8) using the updated value $\Gamma^{n+1}_{i+1/2}$. At the end of each time step the mesh is updated and C is interpolated onto the new mesh using the same linear interpolation scheme as for the velocity in Ref. 51.

The discretization of Eq. (6) is first order accurate in space while both the flow solver and discretization of Eq. (7) are second order in space away from S, and the time update is first order throughout. The method has been validated on several problems of bubble dynamics for both steady and unsteady flows, and good agreement with other theoretical, numerical, and experimental results has been found.

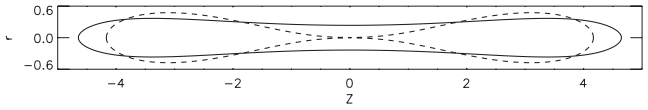

FIG. 1. The solid curve shows the initial prestretched bubble shape $r=R(z,0)$, and the dashed curve shows the bubble shape just before pinch-off when it is free of surfactant and Re=0.17.

III. RESULTS

The initial profile for the simulations consists of a prestretched axisymmetric dumbbell shaped bubble, which is symmetric in the plane $z=0$, where z is an axial coordinate. It is formed by straining a spherical bubble that is centered at the origin in the extensional flow

$$\boldsymbol{u} = \mathrm{Ca}\left(z\boldsymbol{e}_z, -\tfrac{1}{2}r\boldsymbol{e}_r\right), \tag{12}$$

where $\mathrm{Ca}=G/U$ is the capillary number, G is the imposed strain rate, r is a radial coordinate, and $\boldsymbol{e}_r$, $\boldsymbol{e}_z$ are unit vectors in the (outward) radial and axial directions. During the straining motion the surface tension is constant, with $E=0$ in Eq. (10), so that the interface evolves as though it is free of surfactant. The extent of deformation is characterized by the Taylor deformation number

$$D = \frac{L-B}{L+B}, \tag{13}$$

where L and B are the bubble half length in the z-direction and the minimum radius in the r-direction, respectively. The initial profile for the simulations has the shape that is formed with Ca=5.87 and Re=0.17 when the deformation number $D=0.91$, at which instant time is set to $t=0$. This profile $R(z,0)$ is shown by the solid curve in Fig. 1. It has an aspect ratio of $B/L \simeq 0.05$, where B is measured at the minimum radius or neck at $z=0$. The imposed strain and fluid velocity are then instantaneously set to zero, and the bubble evolves in a quiescent flow for $t>0$.

The choice of initial bubble shape is based on the result described by Doshi *et al.*[14] that a surfactant-free bubble that is slender and has an initial profile with a local minimum away from its end points subsequently develops a neck there, the radius of which decreases to zero in finite time so that the bubble profile pinches off under the influence of surface tension. The clean bubble profile at pinch-off is shown by the dashed curve in Fig. 1. The dumbbell shaped initial profile serves as a benchmark for study of the influence of surfactant, and was used in our earlier study.[32]

The qualitative features of pinch-off for a clean bubble are independent of Re for values $\mathrm{Re} \lesssim 1$. Pinch-off occurs at $z=0$ with a single locally parabolic minimum and nonzero interface velocity. Further, the time evolution of the neck radius $R(0,t)$ is found to be nearly independent of Re below $\mathrm{Re} \simeq 0.25$.

A. Thread formation with a soluble surfactant

When the bubble evolves in the presence of surfactant for $t>0$, a notably different behavior can occur relative to the surfactant-free case. This is distinguished by the formation of a thin thread of the interior fluid that may persist for sufficiently large times that it can be considered quasisteady.

In earlier work[32] we noted the formation of a thread in the presence of insoluble surfactant. In this section we consider the influence of a surfactant that is soluble in the exterior fluid, and study how the evolution can change with respect to the three parameters associated with surfactant solubility. These are the surface-to-bulk transfer coefficient J of Eq. (6), the bulk Peclet number Pe of Eq. (7), and the interface partition coefficient K of Eq. (8).

The initial data for the simulations consist of the dumbbell shaped profile of Fig. 1, with $\boldsymbol{u}(\boldsymbol{x},0)=\boldsymbol{0}$ everywhere, and $C(\boldsymbol{x},0)=1$ in the exterior fluid. On the interface $\Gamma(\boldsymbol{x},0)=\Gamma_i$ is constant and $C(\boldsymbol{x},0)=C_i$ is a constant given by Eq. (8). Unless noted otherwise, parameter values used throughout are $\Gamma_i=0.4$, $\mathrm{Re}=0.17$, $E=0.15$, and $\mathrm{Pe}_s=\infty$, where we have applied the commonly used assumption that the ratio of surface diffusion to surface advection of surfactant is sufficiently small so that surface diffusion can be neglected. In all our simulations, the initial surfactant concentration Γ_i is below the equilibrium value, as determined from Eq. (8) and the far-field condition (9). This will be the case for a bubble that is initially spherical and in equilibrium with its surroundings then rapidly stretched to a dumbbell shape and released.

1. Varying J with K and Pe fixed

Change in J with K and Pe fixed corresponds to changing the dimensional surfactant concentration at infinity C_∞ together with the ratio of desorption to adsorption rates κ_2/κ_1 so that $K=\kappa_1 C_\infty/\kappa_2$ of Eq. (8) and all other parameters remain fixed. Since the normal derivative of the bulk surfactant concentration at the bubble surface $\boldsymbol{n}\cdot\nabla C|_S$ stays bounded, in the limit $J\to 0$ Eqs. (7)–(9) become uncoupled from the remainder of the system so that the behavior of an insoluble surfactant is recovered.

Figure 2 shows the results of simulations with $\mathrm{Pe}=10$ and $K=10^2$ at two different values of the transfer coefficient J. In Fig. 2(a) $J=10^{-4}$, which is sufficiently small that the evolution is close to that found for insoluble surfactant. The data show that similar to evolution with insoluble surfactant, at large times a quasisteady thread of the interior fluid forms, which connects two parent bubbles via constrictions or bridges.

The mechanism for thread formation is given by noting that since the interior pressure p_i is less than the capillary pressure $p_c=\sigma/R$ at the neck of the initial profile and when

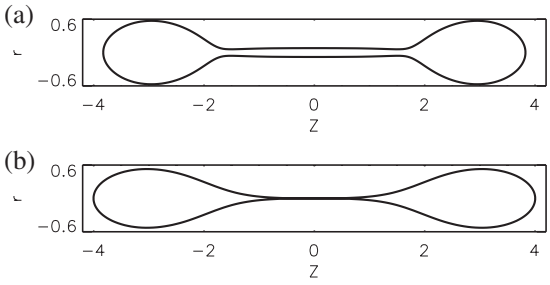

FIG. 2. Evolution with soluble surfactant, $\mathrm{Re}=0.17$, $\Gamma_i=0.4$, $E=0.15$, $\mathrm{Pe}_s=\infty$, $\mathrm{Pe}=10$, and $K=100$. (a) The transfer coefficient $J=10^{-4}$ is sufficiently small for a quasisteady thread to form. (b) The transfer coefficient $J=10^{-2}$ is sufficiently large for pinch-off to occur as in the surfactant-free case in Fig. 1, but the profile has a relatively elongated neck in a neighborhood of the pinch point.

the viscosity ratio λ is small, the exterior fluid undergoes a contraction that is nearly radial in a cylindrical geometry. The contraction causes a local decrease in area of the interface and hence an increase in the surface concentration of surfactant Γ so that from the equation of state, the surface tension decreases. When the effect of surfactant solubility is sufficiently small, the decrease in surface tension during this stage of the evolution is sufficiently rapid relative to the decrease in radius that the capillary pressure σ/R decreases to approach near-equilibrium with the interior pressure p_i before pinch-off can occur. When this near equilibrium is achieved, further contraction almost ceases. A thin thread of the interior fluid then begins to form, propagating outward in the axial direction from $z=0$, as neighboring sections $z=$constant decrease in radius until the local capillary and internal pressure are equal.

At the larger value $J=10^{-2}$ of the simulation shown in Fig. 2(b), the interface pinches off at $z=0$ as in the surfactant-free case (Fig. 1), although as pinch-off is approached the interface near $z=0$ has a more elongated neck than in the surfactant-free example of Fig. 1. The local increase in surface concentration of surfactant Γ that occurs on contracting sections of the interface causes an increase in the neighboring bulk concentration $C|_s$ via Eq. (8), and a gradient of bulk surfactant develops that is directed toward the interface. At this larger value of the transfer coefficient J, surfactant leaves the interface appreciably via the diffusive flux term $J\boldsymbol{n}\cdot\nabla C|_s<0$ of Eq. (6). As a consequence, the decrease in surface tension σ near the bubble neck is no longer sufficiently rapid relative to the decrease in profile radius R for the capillary pressure σ/R to equilibrate with the interior pressure p_i so that surfactant-free-type pinch-off occurs. Nonetheless, enough surfactant remains on the interface near $z=0$ both for pinch-off to be delayed and for the profile to have a more elongated neck or waist relative to the evolution in the surfactant-free case.

The outward normal derivative of the bulk surfactant concentration at the interface $\boldsymbol{n}\cdot\nabla C|_s$ for the simulation of Fig. 2(a) is shown in Fig. 3, at the same time as in Fig. 2(a), for $z\geq 0$. This bears out the interpretation described for the mechanism of thread formation at small J and the elongated neck pinch-off that occurs for larger J. Everywhere on the thin thread (i.e., for $0\lesssim z\lesssim 1.5$), $\boldsymbol{n}\cdot\nabla C|_s<0$ so that soluble

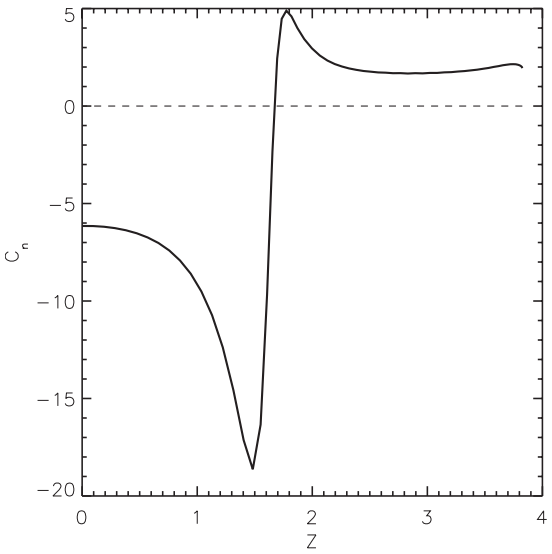

FIG. 3. The outward normal derivative of the bulk surfactant concentration at the interface, $\boldsymbol{n}\cdot\nabla C|_s$, for the simulation of Fig. 2(a). Here $J=10^{-4}$ and thread formation occurs.

surfactant tends, if possible, to desorb from the interface and enter the bulk flow. This is a maximum near the narrowest point of the profile, that is, at the thread constriction, where in Fig. 3 $\boldsymbol{n}\cdot\nabla C|_s \simeq -19$. There is a rapid change in the gradient and its direction is reversed where the constriction meets the parent bubble. However, at the small value of the transfer coefficient $J=10^{-4}$ of this simulation, the exchange of surfactant between the interface and the bulk is sufficiently small for a quasi steady thread to form.

The evolution of the neck radius with time $R(0,t)$ for the data of Fig. 2 is shown in Fig. 4, together with the evolution for the surfactant-free case. This shows the abrupt change from contraction to the onset of thread formation when the transfer coefficient is small ($J=10^{-4}$) and the decrease in the contraction rate before pinch-off when the transfer coefficient is larger ($J=10^{-2}$). Comparison with the surfactant-free

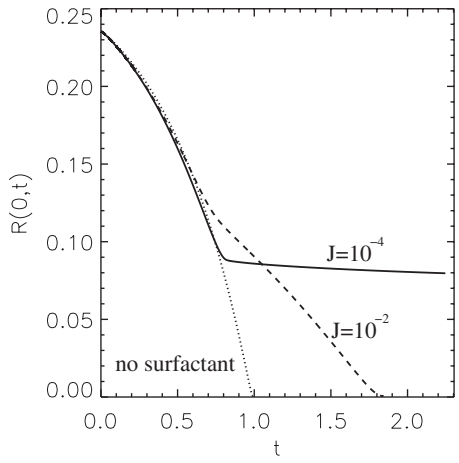

FIG. 4. Bubble neck radius $R(0,t)$ vs time for the same parameter values as in Fig. 2. After its initial stage, contraction almost ceases and thread formation occurs for $J=10^{-4}$ (solid curve), while contraction slows before pinch-off for $J=10^{-2}$ (dashed curve), but continues unabated in the absence of surfactant (dotted curve).

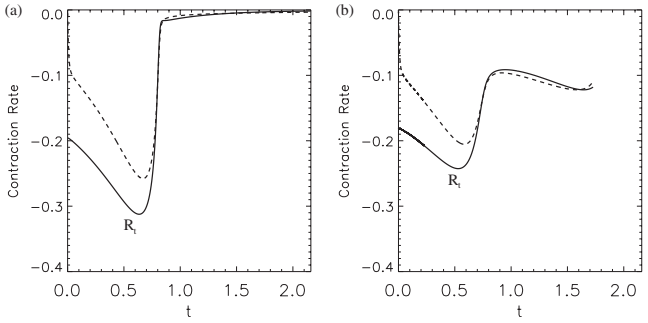

FIG. 5. Contraction rate $\partial_t R(0,t)$ (solid line) and the expression on the right-hand side of Eq. (14) (dashed line) for the data of Fig. 2: (a) $J=10^{-4}$, thread formation; (b) $J=10^{-2}$, pinch-off.

case shows that in its initial stage the contraction rate is almost independent of the influence of surfactant.

In Sec. IV we describe a long-wave model for the dynamics of a periodic capillary jet which predicts very similar behavior to that found here for a contracting bubble. The agreement is due in part to the small aspect ratio of the initial bubble profile and the minor role of end effects. If the initial aspect ratio of jet radius to axial half wavelength in the long-wave model is $\epsilon(0<\epsilon\ll 1)$ then the interface radius is $r=\epsilon R(z,t)$, and the ϵ-scaled radius R satisfies

$$\frac{\partial R}{\partial t}=\frac{R}{2}\left(p_i-\frac{\sigma}{R}\right). \tag{14}$$

Like the mechanism for quasisteady thread formation just described, this has a steady thread radius when the internal and capillary pressures are equal. The extent of agreement between the long-wave model and the numerical simulations is indicated in Fig. 5, which shows the contraction rate $\partial_t R(0,t)$ and the right-hand side of Eq. (14) at $z=0$ taken from the simulation data of Fig. 2. The two expressions agree to within 10% or less for all times after the initial stage of contraction, $t\gtrsim 0.75$, and Fig. 5(a), with $J=10^{-4}$, shows that the thread radius at $z=0$ is nearly steady for $t\gtrsim 1.5$

2. Varying Pe with J and K fixed

Change in the bulk Peclet number Pe with J and K fixed is equivalent to a change in both the diffusivity of surfactant in the suspending fluid D and the saturated concentration of adsorbed surfactant Γ_∞, with Γ_∞/D and other parameters fixed. For this set of simulations, $J=10^{-4}$ and $K=20$. At this smaller value of K, relative to the value $K=100$ of the previous set, the rate of desorption from the interface is enhanced.

Figure 6(a) shows the neck radius $R(0,t)$ versus time. The decrease in neck radius is almost independent of Pe during the initial stage of contraction, but this is interrupted at $t\simeq 0.75$ when a thread begins to form in a neighborhood of $z=0$, and the subsequent reduction in contraction rate is less at larger values of Pe. This is seen more clearly in the close up of Fig. 6(b) for times $t\gtrsim 0.8$.

The increase in contraction rate with Peclet number for times $t\gtrsim 0.8$ is caused by the ability of the suspending fluid to support larger gradients of bulk surfactant C when diffu-

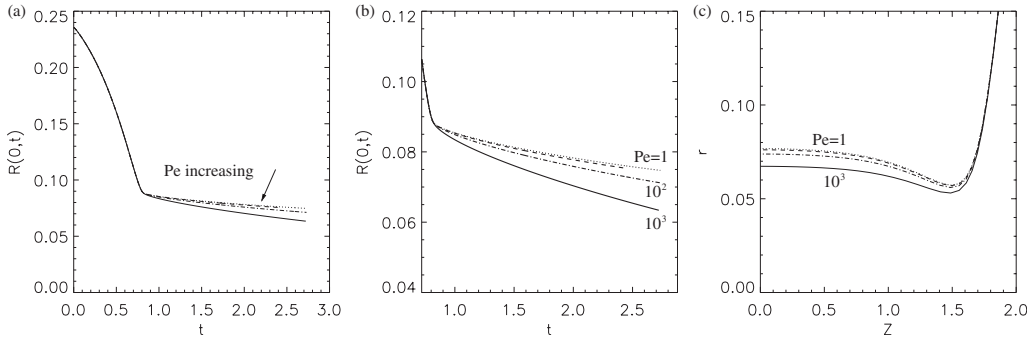

FIG. 6. Evolution with $J=10^{-4}$ and $K=20$ fixed at different values of $\mathrm{Pe}=10^0$ (dotted line), 10^1 (dashed line), 10^2 (broken line), and 10^3 (solid line). (a) The neck radius $R(0,t)$ vs t. In each case a quasisteady thread forms. (b) Close up of (a). (c) Thread radius $R(z,t)$ vs z at time $t=2.3$.

sion is small. During the initial stage of contraction (for times $t \lesssim 0.75$) the increase in adsorbed surfactant Γ due to local decrease in surface area at the neck increases the amount of bulk surfactant immediately adjacent to the interface $C|_s$, according to Eq. (8), to a value above the far-field concentration $C=1$. Surfactant then begins to desorb from S, and at large values of Pe the suspending fluid supports a narrow transition layer of bulk surfactant adjacent to S. This has increased normal gradient $|\boldsymbol{n}\cdot\nabla C|_S$ and hence enhanced desorption from the interface occurs as expressed by the term $J\boldsymbol{n}\cdot\nabla C|_S<0$ in Eq. (6). The increase in desorption increases the capillary pressure, causing an increase in contraction rate. Figure 6(c) shows thread profiles for the same values of Pe as in Figs. 6(a) and 6(b) at time $t=2.3$. In each case, the thread profile shows the formation of a constriction where the thread joins the parent bubble, but this is less conspicuous at larger Pe.

The occurrence of increased capillary pressure at larger Peclet number during the stage of thread formation, which leads to smaller thread radius, also leads at times $t \gtrsim 1.5$ to smaller values of the surface tension on the thread via increased concentration of adsorbed surfactant caused by smaller thread surface area. This is seen in Fig. 7(a), which shows the surface tension $\sigma(0,t)$ at $z=0$ versus t. At all values of Pe in this set of simulations, the desorption of surfactant is sufficient that the quasisteady thread is expected to be driven to pinch-off at larger times, probably at the thread end constriction. This is borne out both by the simulation data for the contraction rate at the neck $\partial_t R(0,t)$ and by the expression on the right-hand side of Eq. (14) at $z=0$, which is shown in Fig. 7(b). The data show that the contraction rate is always negative and approaches a steady nonzero value at times $t \gtrsim 2.3$.

Concentration profiles of surfactant close to the interface at the end of the simulation are shown in Fig. 8 with the same values of $J=10^{-4}$ and $K=20$ as in Figs. 6 and 7. The data confirm that the surface value $C|_s$ on the thread is above the far-field value $C=1$ so that surfactant desorbs from the thread and diffuses into the bulk, while on the parent bubble $C|_s$ is below the far-field value and surfactant adsorbs. At the larger Peclet number $\mathrm{Pe}=10^3$ of Fig. 8(b) the bulk surfactant gradient is confined closer to a neighborhood of the interface and is larger at the interface itself so that surfactant exchange between the interface and the bulk is enhanced, while at the

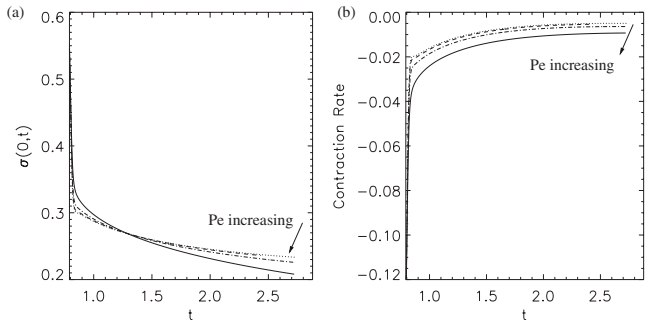

FIG. 7. Evolution with the same parameter values as in Fig. 6 (and with the same line styles for $\mathrm{Pe}=10^0$, 10^1, 10^2, and 10^3). (a) Surface tension at the neck $\sigma(0,t)$ vs t. (b) Contraction rate given by the right-hand side of Eq. (14) at $z=0$ vs t.

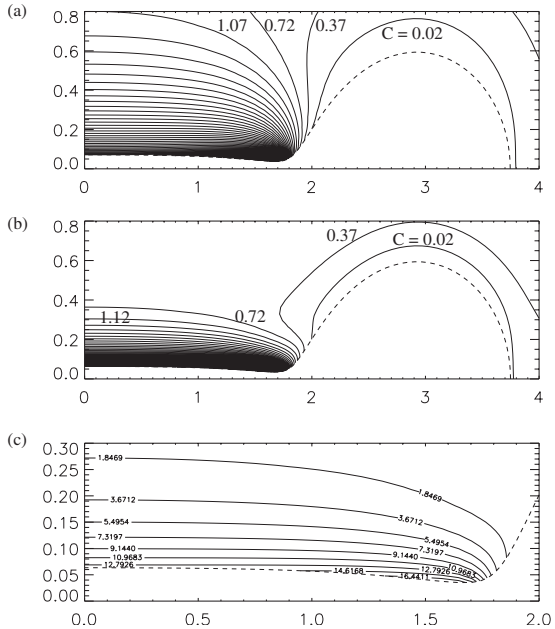

FIG. 8. Concentration profiles of surfactant close to the interface at the end of the simulation, with the same parameter values $J=10^{-4}$ and $K=20$ as in Figs. 6 and 7. Surfactant desorbs from the thread and adsorbs onto the parent bubble. (a) $\mathrm{Pe}=10^2$, exchange between the interface and bulk is relatively small. (b) $\mathrm{Pe}=10^3$, the normal gradient of bulk surfactant concentration at the interface increases so that surfactant exchange between the phases is enhanced. (c) Close up of (b) near the quasisteady thread.

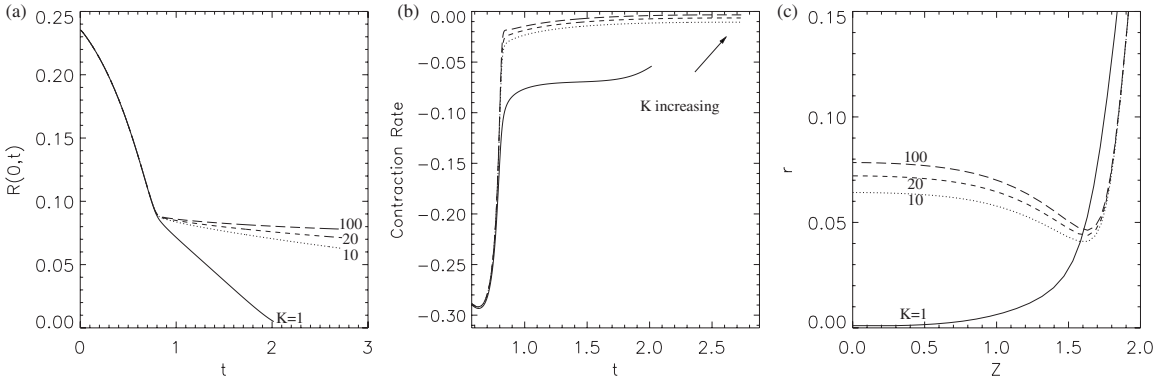

FIG. 9. Evolution with $J=10^{-4}$ and $\mathrm{Pe}=10^{2}$ at different values of $K=1$ (solid line), 10 (dotted line), 20 (short-dashed line), and 100 (long-dashed line). (a) Neck radius $R(0,t)$ vs time t. (b) Contraction rate given by right-hand side of Eq. (14) at $z=0$ vs t. (c) Profiles $r=R(z,t)$ vs z; $K=1$ near pinch-off at time $t=2.16$, and for $K=10$, 20, and 100 at time $t=2.6$.

lower Peclet number $\mathrm{Pe}=10^{2}$ of Fig. 8(a), diffusion persists further away from the interface and is relatively small at the interface itself. At both values of the Peclet number, desorption is most significant at the thread end constriction.

3. Varying K with J and Pe fixed

For a spherical drop in equilibrium with no flow, the present choice of nondimensional variables implies that $C=1$ everywhere, and in particular $C|_s=1$. The equilibrium value of adsorbed surfactant Γ_{eq} is given by Eq. (8), which shows that at large K, that is at a large rate of adsorption relative to desorption, the equilibrium value of Γ is also relatively large. Conversely, at small K surfactant desorbs more readily and the equilibrium value of Γ is small. In this way the limits of large and small K correspond to surfactant that is only slightly soluble in the bulk flow and to surfactant that is highly soluble, respectively. In the latter case the interface evolves as though it is more nearly surfactant-free.

Evolution of the neck radius $R(0,t)$ with $J=10^{-4}$ and $\mathrm{Pe}=10^{2}$ is shown in Fig. 9(a). During the initial stage of contraction, for times $t\lesssim 0.75$, there is no noticeable difference in the dynamics throughout the range of K considered. At later times, for the smallest value of K considered, $K=1$, there is no stage of quasisteady thread formation. Relative to the completely surfactant-free case (see Fig. 1), for which pinch-off occurs when $t\simeq 1.0$, the neck contraction rate is reduced and the neck pinches off at $z=0$ with a more elongated neck, which is shown in Fig. 9(c) at $t\simeq 2.2$.

In contrast, when $K=100$ a persistent quasisteady thread forms, which has constrictions at its ends and a profile that is shown at time $t=2.6$ in Fig. 9(c). At this time, the contraction rate at $z=0$, as given by the right-hand side of Eq. (14) and shown in Fig. 9(b), is close to zero, $|\partial_t R(0,t)|\simeq 0.003$. At still later times, the thread continues to extend in length and narrows more at the thread end constrictions, and it is expected that it ultimately pinches off there.

Data for intermediate values of $K=10$ and $K=20$ are also given in Figs. 9(a)–9(c), and show the formation of a quasisteady thread with end constrictions. However, since the surfactant can desorb more easily at these lower values of K relative to the case $K=100$, the concentration of adsorbed surfactant on the thread is smaller, with the result that the capillary pressure is always slightly in excess of the interior pressure, as is seen in the data for the contraction rate of Fig. 9(b), and the thread radius continues to decrease slowly in time throughout its length. It appears that at the chosen values of J and Pe for this set of simulations, pinch-off occurs first at the constrictions for all $K\geq 10$, but at smaller $K<10$ the thread's lifetime is increasingly short and there is a threshold value of K below which pinch-off occurs first at $z=0$, as found for $K=1$.

4. Varying Pe and J with K and χ fixed

Change in Pe and J with K and χ fixed is equivalent to a change in the diffusivity D of the bulk surfactant concentration, with small D corresponding to large Pe and, from Eq. (11), $J=O(\mathrm{Pe}^{-1})$ as $\mathrm{Pe}\to\infty$. This introduces two potentially competing effects. As noted in Sec. III A 2, at large bulk Peclet number large gradients of bulk surfactant can be sustained adjacent to the interface, thereby increasing the normal gradient $|\boldsymbol{n}\cdot\nabla C|_S=O(\mathrm{Pe}^{1/2})$ and promoting thread pinch-off caused by surfactant entering the bulk flow from the interface. On the other hand, the influence on the net exchange of surfactant at the interface is expressed by the term $J\boldsymbol{n}\cdot\nabla C|_S$ in Eq. (6), which is reduced by the decrease in the transfer coefficient J and is of order $O(\mathrm{Pe}^{-1/2})$. This tends to reduce the influence of solubility, promoting quasisteady thread formation at large Pe, and this is the effect that prevails here.

Data from simulations with $\chi=0.005$ and $K=20$ at different Pe, from $\mathrm{Pe}=10^{0}$ (i.e., $J=10^{-1}$) to $\mathrm{Pe}=10^{3}$ (i.e., $J=10^{-4}$) are shown in Figs. 10–12. Figure 10(a) shows the neck radius $R(0,t)$ versus time. At the largest value of Pe considered, the initially rapid contraction of the neck is interrupted at $t\simeq 0.75$ and is followed by a stage of quasisteady thread formation centered on $z=0$, while for smaller values of $\mathrm{Pe}\leq 10^{2}$ there is no identifiable thread formation and the profile pinches off at $z=0$. The quarter profiles $r=R(z,t)$ for $z\geq 0$ at time $t=1.51$ are shown in Fig. 10(b), an instance that is just before pinch-off for the two smaller values of $\mathrm{Pe}\leq 10^{1}$. The slow evolution of the neck radius at $\mathrm{Pe}=10^{3}$ is seen in the data for the neck contraction rate $\partial_t R(0,t)$ of Fig. 10(c), which approaches a small but nonzero value for times $t\gtrsim 2.3$. Data for this case ($\mathrm{Pe}=10^{3}$, $J=10^{-4}$, $K=20$) were

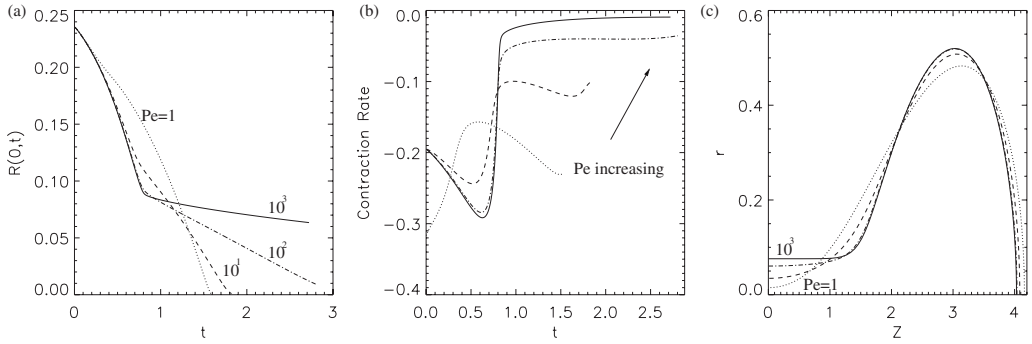

FIG. 10. Evolution with $\chi=0.005$ and $K=20$ at different Pe$=10^0$ (dotted line), 10^1 (dashed line), 10^2 (broken line), and 10^3 (solid line) with $J=\chi K/\mathrm{Pe}$. (a) Neck radius $R(0,t)$ vs time. The three smaller values of Pe show pinch-off, whereas Pe$=10^3$ shows thread formation. (b) Profiles $r=R(z,t)$ at time $t=1.51$. (c) Contraction rate, given by the right-hand side of Eq. (14) at $z=0$, vs t.

presented earlier in Figs. 6(a)–6(c) (solid line) so that while the thread profile at time $t=1.51$ of Fig. 10(b) is flat, that is, not constricted at its ends $z\simeq\pm1.1$, at the later time $t=2.3$ of Fig. 6(c) the thread ends have extended outward to $z\simeq\pm1.5$ and have developed constrictions where they join the parent bubbles.

Data for the total amount of surfactant on the evolving interface S are shown in Fig. 11(a), and data for the total amount of surfactant averaged by the area of S are shown in Fig. 11(b). Figure 11(a) shows that at the largest value of Pe$=10^3$, and thus the least effective exchange of surfactant between the interface and the bulk, the total surfactant coverage on S is almost constant in time, although there is a slight initial rise followed by a subsequent fall when the quasisteady thread develops. This change is more noticeable at smaller Pe. With the initial surface coverage $\Gamma_i=0.4$ and $K=20$ of these simulations, $C|_S(t=0)=0.03$, and there is an initial uptake of adsorbed surfactant Γ from the bulk everywhere on S. This increase in Γ is augmented by radial contraction in the region of the narrowing neck, and is sufficient at the smallest value of Pe$=10^0$ to significantly decrease the local contraction rate due to the decrease in surface tension, as seen in Fig. 10(a) at time $t\simeq0.3$. At later times the local concentration of surfactant is sufficiently large in a neighborhood of $z=0$ that the direction of exchange with the bulk is reversed, leading to the subsequent fall in surfactant coverage seen in Fig. 11(a), and which occurs at time $t\simeq0.7$ for Pe$=10^0$.

When contraction to either pinch-off or thread formation occurs there is a decrease in the total area of S during the later stages of evolution, and the surface-averaged surfactant coverage $\langle\Gamma\rangle$ shown in Fig. 11(b) either continues to increase or approaches a constant. At the smallest value of Pe$=10^0$, diffusion in the bulk is sufficiently fast and exchange with the interface is sufficiently effective that the surface-averaged coverage approaches the equilibrium value $\Gamma_{\mathrm{eq}}\simeq0.95$ at time $t\simeq1.0$ before pinch-off occurs. At the larger values of Pe of this simulation, exchange of surfactant is less effective and the averaged coverage continues to increase but at a slower rate. Desorption of surfactant from a nearly quasisteady thread is small and most noticeable at thread end constrictions or in a neighborhood of a pinch point, whereas elsewhere on S surfactant is taken up from the bulk and the surface-averaged value increases toward Γ_{eq}.

This is borne out by data for the adsorbed surfactant concentration profiles $\Gamma(z,t)$ shown in Fig. 12. At the smaller bulk Peclet number Pe$=10^0$ of Fig. 12(a) surfactant is initially adsorbed via diffusion from the bulk phase everywhere on the interface, but combined with increase due to local contraction, Γ first increases above the equilibrium value $\Gamma_{\mathrm{eq}}\simeq0.95$ at the neck $z=0$ at time $t\simeq0.5$, and in the final

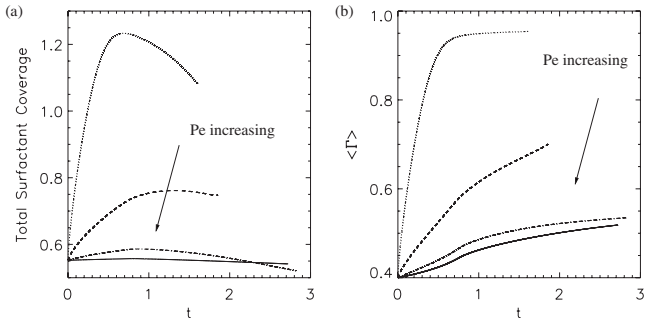

FIG. 11. Evolution with the same parameter values and line styles for the different values of Pe as in Fig. 10. (a) The total surfactant coverage on the interface vs time. (b) The total surfactant coverage averaged by interface surface area vs time.

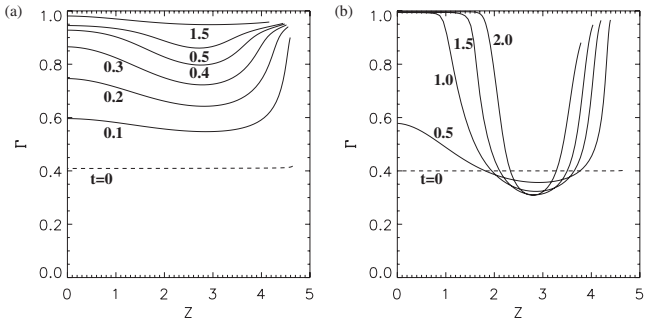

FIG. 12. Evolution with the same parameter values as in Fig. 10, showing surfactant concentration profiles $\Gamma(z,t)$ vs z at times indicated. (a) Bulk Peclet number Pe$=10^0$, pinch-off ($J=10^{-1}$, $K=20$). (b) Bulk Peclet number Pe$=10^3$; thread formation ($J=10^{-4}$, $K=20$).

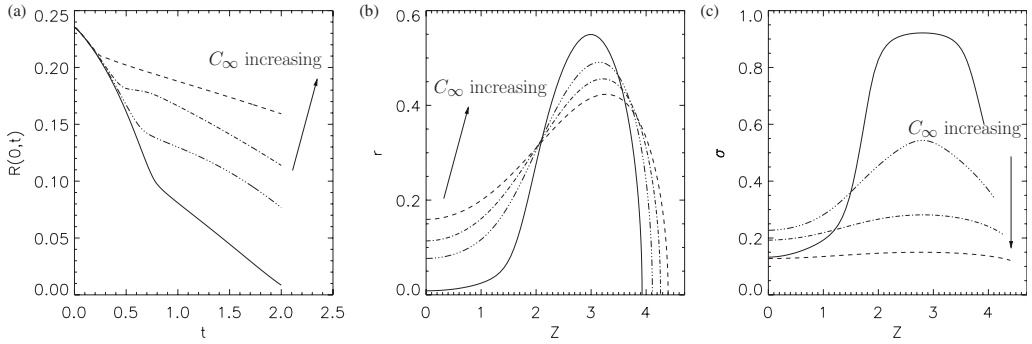

FIG. 13. Evolution with $\mathrm{Pe}=10^2$ and $J/K=\chi/\mathrm{Pe}=1.25\times10^{-4}$ fixed at different values of C_∞. With increasing C_∞, $K=20$ (solid line), $K=100$ (long dot-dashed line), $K=200$ (dot-dashed line), and $K=400$ (dashed line). (a) Neck radius $R(0,t)$ vs time. (b) Profiles $r=R(z,t)$ at time $t=2$. (c) Surface tension on the evolving interface at time $t=2$.

stage of evolution toward pinch-off the direction of exchange with the bulk is reversed almost everywhere on S. At the larger bulk Peclet number $\mathrm{Pe}=10^3$, initial adsorption via diffusion from the bulk is again first reversed at $z=0$ when at time $t\simeq0.75$ a quasisteady thread begins to form. At later times surfactant dissolves from the interface to enter the bulk along the thread but continues to adsorb elsewhere on the parent bubbles where $\Gamma<\Gamma_{\mathrm{eq}}$ although exchange is always small due to the lower value of $J=10^{-4}$.

5. Varying C_∞ with Pe fixed

Both the transfer coefficient J and the partition coefficient K are directly proportional to the bulk surfactant concentration at infinity C_∞ so that change in C_∞ with other parameters fixed corresponds to change in J and K with J/K fixed and the bulk Peclet number Pe fixed.

In Sec. III A 1 it was found that an increase in J alone from 10^{-4} to 10^{-2} with $\mathrm{Pe}=10$ and $K=100$ fixed causes the evolution to change from thread formation to pinch-off. On the other hand, as found in Sec. III A 3, an increase in K alone from 1 to 100 with $J=10^{-4}$ and $\mathrm{Pe}=10^2$ fixed causes a change from pinch-off to thread formation. Here, an increase in C_∞ alone tends to enhance surfactant adsorption to the interface via diffusion from the bulk flow at earlier times during the evolution, and at large C_∞ causes an interval of quasisteady thread formation with large thread radius.

Data from simulations with $\mathrm{Pe}=10^2$ and different values of C_∞ with other parameters fixed are shown in Fig. 13. Figure 13(a) shows the neck radius $R(0,t)$ versus time. At the largest value of C_∞ considered, the initially rapid contraction of the neck is interrupted at $t\simeq0.3$ and is followed by a phase of much slower neck contraction. For smaller C_∞ the transition to slower contraction occurs at later times and the bubble pinches off around $t\simeq2.1$ for the smallest value of C_∞. Quarter profiles $r=R(z,t)$ for $z\geq0$ at time $t=2$ are shown in Fig. 13(b). The slow contraction and large thread radius at large C_∞ are due to significant adsorption of surfactant from the bulk, which causes reduction in the surface tension to a small, near-uniform value. This is seen at the end of the simulation in Fig. 13(c).

The total amount of surfactant on the evolving interface S is shown in Fig. 14(a) and its surface-averaged value is shown in Fig. 14(b). Figure 14(a) shows that at the largest value of C_∞ the total surfactant coverage saturates at $t\simeq0.3$ when the slow neck contraction phase begins, at which time the surface tension is near uniform and $\sigma\simeq0.15$, i.e., slightly above the minimum surface tension σ_{min}. During the remainder of the slow neck contraction phase the total surfactant coverage decreases slightly while its surface-averaged value remains constant. Although there is slight desorption of surfactant from the region of the neck, where $\boldsymbol{n}\cdot\nabla C|_S\simeq-0.1$, the decrease in total coverage is due mostly to slight decrease in the interfacial area. The averaged value $\langle\Gamma\rangle\simeq0.995$ is below but within 2% of the equilibrium value Γ_{eq}.

At smaller values of C_∞ the approach to such an equilibrium state is increasingly slow, and at the smallest value of these simulations the bubble pinches off at the neck long before equilibrium can be reached (solid lines in Figs. 13 and 14). In this case the increase in total surfactant coverage is reversed at time $t\simeq1.0$, and the evolution of the profile toward pinch-off is similar to that for $(J,K,\mathrm{Pe})=(10^{-2},10^2,10^1)$ in Fig. 4 (dashed line).

IV. LONG-WAVE MODELS FOR A CAPILLARY JET WITH SOLUBLE SURFACTANT

The small aspect ratio of the initial bubble profile for the simulations of Sec. III was noted below Eq. (13), see Fig. 1, where the initial profile aspect ratio $B/L\simeq0.05$. If the behavior near the bubble ends is neglected, the evolution is similar to that of a cylindrical capillary jet. For Stokes flow, this can be modeled using a long-wave or slender body approxima-

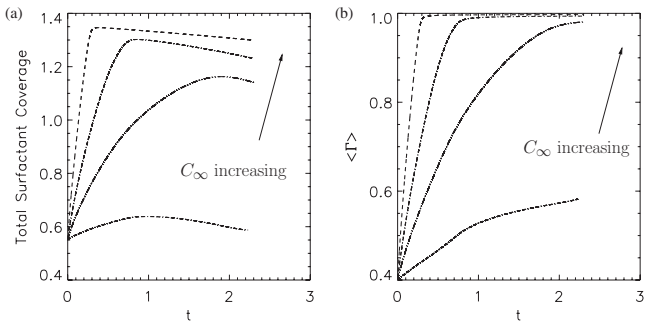

FIG. 14. Evolution with the same parameter values as in Fig. 13. (a) The total surfactant coverage on the interface vs time. (b) The surface-averaged coverage vs time.

tion, with spatially periodic boundary conditions and initial conditions that mimic the initial profile between its sections of maximum radius.

Long-wave equations for the breakup of a capillary jet of small or zero interior viscosity have been derived and analyzed before. For example, the dynamics of a jet that is free of surfactant was investigated thoroughly by Sierou and Lister[17] and the limit of an inviscid jet was studied by Basaran[4] and Suryo *et al.*,[18] while Hameed *et al.*[32] presented long-wave equations for a nearly inviscid or inviscid jet that is coated with insoluble surfactant. Here we extend the results for a surfactant-coated inviscid jet to include the effects of surfactant solubility.

In this section, lengths are made nondimensional by the axial half length l, while the average initial jet radius b is the length scale relevant to the radius' evolution and time scale. With $\epsilon=b/l\ll 1$ as the aspect ratio, this introduces the interface position $r=\epsilon R(z,\tau)$ and time $t=\epsilon\tau$. The interior pressure is also rescaled to $\tilde{p}_i=p_i/\epsilon=O(1)$. Since details of the scalings and derivation of long-wave equations for evolution with insoluble surfactant were given in Ref. 32, here we review the main results.

When line distributions of mass sources $g(z,\tau)$ and Stokeslets $f(z,\tau)$ are introduced, the velocity components are given at leading order by $u\simeq 2g/r$ and $v\simeq 2\ln(1/\epsilon)(2f-\partial_z g)$, where higher order corrections are smaller by a factor of $1/\ln(1/\epsilon)$. The kinematic condition at the interface implies that $u\simeq\partial_\tau R$ on $r=\epsilon R$, which determines $2g\simeq\epsilon R\partial_\tau R$. It turns out that the Stokeslet distribution f appears in the leading order dynamics only in the tangential stress balance and that $f=O(\epsilon)$. As a consequence the Stokeslet distribution, the Marangoni term, and the axial velocity do not contribute to a closed system of long-wave equations at leading order. Simplified expressions for the velocity components (u,v) can be found, and the expression for f is needed to find v. Together with the expression above for g and the result of the normal stress balance at Eq. (16) below, these are

$$u\simeq\epsilon\frac{R\partial_\tau R}{r},\quad v\simeq\epsilon\ln(1/\epsilon)\frac{\partial}{\partial z}\left(\frac{\sigma R}{2}\right). \tag{15}$$

These expressions hold with or without the presence of surfactant, and show that at the interface and within an ϵ-neighborhood in r, $u=O(1)$ while $v=O[\epsilon\ln(1/\epsilon)]$ everywhere.

The results of earlier studies[14,17,18] imply that the normal stress balance, the kinematic condition, and conservation of volume of an inviscid jet are approximated by

$$\frac{\partial R}{\partial\tau}=\frac{R}{2}\left(\tilde{p}_i-\frac{\sigma}{R}\right), \tag{16}$$

$$\tilde{p}_i=\frac{1}{2}\int_{-1}^{1}\sigma R dz. \tag{17}$$

In the presence of surfactant, a surface equation of state, such as Eq. (10), is appended, and the evolution of adsorbed surfactant (6) is approximated by[32]

$$\frac{\partial\Gamma}{\partial\tau}+\frac{\partial_\tau R}{R}\Gamma=\frac{1}{\overline{\mathrm{Pe}}_s}\frac{1}{R}\frac{\partial}{\partial z}\left(R\frac{\partial\Gamma}{\partial z}\right)+\left.\epsilon J\frac{\partial C}{\partial r}\right|_S.$$

The advective flux has been omitted since it is a higher order effect, while the component of the normal motion of the interface and curvature in the radial direction alone are included. The surface Peclet number has been rescaled by setting $\mathrm{Pe}_s=\epsilon\overline{\mathrm{Pe}}_s$ to retain the influence of surface diffusion, although values for real fluid systems suggest that this effect may be negligible. The small aspect ratio approximation implies that the outward normal derivative of the surfactant exchange term is approximated by its radial component.

Expression (15) for the velocity components implies that the evolution of bulk surfactant (7) is approximated by

$$\frac{1}{\epsilon}\frac{\partial C}{\partial\tau}+\epsilon\frac{R\partial_\tau R}{r}\frac{\partial C}{\partial r}+\epsilon\ln(1/\epsilon)\frac{\partial}{\partial z}\left(\frac{\sigma R}{2}\right)\frac{\partial C}{\partial z}=\frac{1}{\mathrm{Pe}}\nabla^2 C \tag{18}$$

for $r>\epsilon R(z,\tau)$, where since $r=O(\epsilon)$ near the interface, the axial advective flux is higher order. Two simplifications that lead to closed leading order models can now be identified in the limits of small and large bulk Peclet number Pe.

When the Peclet number is small like $\mathrm{Pe}=o(\epsilon)$, bulk diffusion of surfactant is sufficiently fast to be almost instantaneous. This limit was considered in the context of a viscous drop strained in an extensional flow by Milliken and Leal[40] and a buoyant translating drop by Johnson and Borhan.[41] The leading order bulk surfactant concentration satisfies Laplace's equation with the boundary conditions (8) and (9). Its solution can be described in terms of a line distribution of sources $h(z,\tau)$ on the axis $r=0$ by using the three-dimensional Green's function as

$$C=1-\int_{-1}^{1}\frac{h(\xi,\tau)d\xi}{[r^2+(z-\xi)^2]^{1/2}}.$$

Expansion of the integral as $r\to 0$ shows that $C=1+2h(z,\tau)\ln r+O(h)$ so that the interface boundary condition implies that

$$h=\frac{1-C|_s}{2\ln(1/\epsilon)}+O[\ln^{-2}(1/\epsilon)]$$

and

$$C=1+\frac{1-C|_s}{\ln(1/\epsilon)}\ln r+O[\ln^{-1}(1/\epsilon)]. \tag{19}$$

In the far field, $C-1=O(r^{-1})$ as $r\to\infty$.

From Eqs. (8) and (19), the normal derivative of C on S is

$$\boldsymbol{n}\cdot\nabla C|_s=\frac{1}{\epsilon\ln(1/\epsilon)}\left[1-\frac{\Gamma}{K(1-\Gamma)}\right]\frac{1}{R}+O[\epsilon\ln^{-2}(1/\epsilon)].$$

In terms of a rescaled transfer coefficient $\bar{J}=O(1)$, given by $J=\bar{J}\ln(1/\epsilon)$, the equation for evolution of adsorbed surfactant in the small bulk Peclet number limit is therefore

$$\frac{\partial\Gamma}{\partial\tau}+\frac{\partial_\tau R}{R}\Gamma=\frac{1}{\overline{\mathrm{Pe}}_s}\frac{1}{R}\frac{\partial}{\partial z}\left(R\frac{\partial\Gamma}{\partial z}\right)+\frac{\bar{J}}{R}\left(1-\frac{\Gamma}{K(1-\Gamma)}\right). \tag{20}$$

When the Peclet number is large like $\mathrm{Pe}=\overline{\mathrm{Pe}}/\epsilon$ with $\overline{\mathrm{Pe}}=O(1)$, a narrow transition layer in C develops adjacent to the interface. Setting $r=\epsilon\bar{r}$ with $\bar{r}=O(1)$ in Eq. (18) gives the ϵ-independent reduced equation

$$\frac{\partial C}{\partial \tau}+\frac{R\partial_\tau R}{\bar{r}}\frac{\partial C}{\partial \bar{r}}=\frac{1}{\overline{\mathrm{Pe}}}\left(\frac{\partial^2}{\partial \bar{r}^2}+\frac{1}{\bar{r}}\frac{\partial}{\partial \bar{r}}\right)C \tag{21}$$

for $\bar{r}>R(z,\tau)$. The boundary conditions for C are Eq. (8) at the interface and Eq. (9) as $\bar{r}\to\infty$. In terms of an interface-centered radial coordinate $s=\bar{r}-R(z,\tau)$, the time derivative transforms like $\partial_\tau \mapsto \partial_\tau-(\partial_\tau R)\partial_s$ to give

$$\frac{\partial C}{\partial \tau}-\frac{\partial_\tau R}{R+s}s\frac{\partial C}{\partial s}=\frac{1}{\overline{\mathrm{Pe}}}\left(\frac{\partial^2}{\partial s^2}+\frac{1}{s}\frac{\partial}{\partial s}\right)C \tag{22}$$

for $s>0$. The evolution of Γ in this limit is given by

$$\frac{\partial \Gamma}{\partial \tau}+\frac{\partial_\tau R}{R}\Gamma=\frac{1}{\overline{\mathrm{Pe}}_s}\frac{1}{R}\frac{\partial}{\partial z}\left(R\frac{\partial \Gamma}{\partial z}\right)+\left.J\frac{\partial C}{\partial s}\right|_s. \tag{23}$$

To summarize, we have formed leading order long-wave models for the evolution of an inviscid capillary jet in limits of small and large bulk Peclet number of soluble surfactant. In both cases, the governing equations include Eqs. (16) and (17), which also hold in the surfactant-free case, and an equation of state, which we take to be Eq. (10). For small bulk Peclet number $[\mathrm{Pe}=o(\epsilon)]$ the system is closed by a fourth equation, Eq. (20) for the evolution of adsorbed surfactant, whereas for large bulk Peclet number $[\mathrm{Pe}=O(\epsilon^{-1})]$, the evolution of adsorbed surfactant is given by Eq. (23) with a fifth Eq. (22) for bulk surfactant adjacent to the interface. Boundary conditions are periodicity in z at $z=\pm 1$, and for C, Eq. (8) on the interface and Eq. (9) as $s\to\infty$.

A linear stability analysis of the long-wave models, for disturbances to a constant radius cylindrical jet with uniform surface and bulk surfactant concentrations that are in equilibrium, agrees with the long-wave expansion of the characteristic equation for linear stability found by Hansen *et al.*[26] If undisturbed or basic state values are denoted by an $*$ subscript, then in terms of the radius R_* and surface concentration Γ_*,

$$\sigma_*=\sigma(\Gamma_*),\quad \tilde{p}_{i*}=\frac{\sigma_*}{R_*},\quad C_*=\frac{\Gamma_*}{K(1-\Gamma_*)}. \tag{24}$$

Normal mode disturbances of the long-wave models that are proportional to $e^{ikz+\omega t}$ have growth rate ω that satisfies

$$\left(\omega-\frac{\sigma_*}{2R_*}\right)\left(\omega+\frac{k^2}{\overline{\mathrm{Pe}}_s}+\mathcal{S}\right)-\omega\frac{\sigma'(\Gamma_*)\Gamma_*}{2R_*}=0, \tag{25}$$

where $\mathcal{S}$ represents the influence of surfactant solubility, given by

$$\mathcal{S}=\begin{cases}\dfrac{\bar{J}}{R_*K(1-\Gamma_*)^2} & \text{when } \mathrm{Pe}=o(\epsilon),\\ \dfrac{J}{K(1-\Gamma_*)^2}\dfrac{mK_1(mR_*)}{K_0(mR_*)} & \text{when } \mathrm{Pe}=\overline{\mathrm{Pe}}/\epsilon.\end{cases} \tag{26}$$

Here $\bar{J}$ is the $O(1)$ rescaled version of the transfer coefficient J defined above Eq. (20), while $K_n(z)$ is the modified Bessel function of the third kind (of order n) and $m=(\omega\,\overline{\mathrm{Pe}})^{1/2}$.

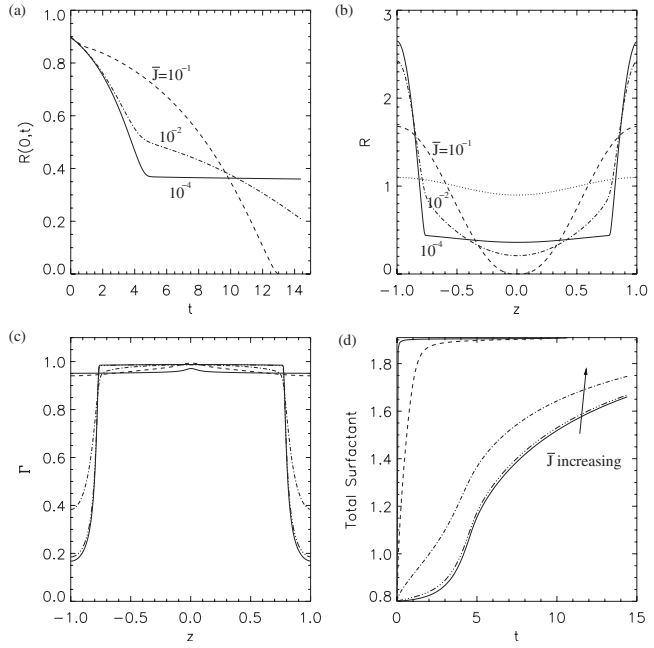

FIG. 15. Solution of the long-wave model in the limit of small bulk Peclet number Pe, with $K=10^3$ and $\overline{\mathrm{Pe}}_s=\infty$, at different values of $\bar{J}$: $\bar{J}=1$ (thin solid line), $\bar{J}=10^{-1}$ (dashed line), $\bar{J}=10^{-2}$ (dot-dashed line), $\bar{J}=10^{-3}$ (dot-dot-dot-dashed line), and $\bar{J}=10^{-4}$ (thick solid line). (a) Neck radius $R(0,t)$ vs time t. (b) Profiles $r=R(z,t)$ at the end of each simulation. (c) The corresponding surfactant concentration profiles $\Gamma(z,t)$. (d) The total surfactant coverage vs time.

In the absence of surfactant solubility $\mathcal{S}=0$ and Eq. (25) reduces to the stability results for an inviscid capillary jet coated with insoluble surfactant. Without surface diffusion there is one marginally stable branch and one branch that is unstable (stable) when $\sigma_*>-\sigma'(\Gamma_*)\Gamma_*[\sigma_*<-\sigma'(\Gamma_*)\Gamma_*]$. For large bulk diffusion of surfactant $[\mathrm{Pe}=o(\epsilon)]$, Eq. (25) has two roots in the ω-plane whose product is negative so that surfactant solubility guarantees an unstable branch and the inviscid capillary jet is always unstable to small perturbations. Thus bulk diffusion of surfactant ensures that the inviscid capillary jet is always unstable, even though it may be stable in the absence of surfactant solubility.

A. Numerical solution of the long-wave model: Small bulk Peclet number $\mathrm{Pe}=o(\epsilon)$

In this subsection we present the results of numerical integration of the long-wave equations for $\mathrm{Pe}=o(\epsilon)$ using a finite-difference method. For comparison with results of the direct numerical simulations, the same parameter values are used throughout, i.e., $E=0.15$, $\overline{\mathrm{Pe}}_s=\infty$, and the initial surfactant coverage $\Gamma_i=0.4$. The initial profile is given by $R(z,0)=a-\sqrt{2(1-a^2)}\cos(\pi z)$ with $a=0.9888$ to give a dumbbell shaped perturbation from a cylindrical jet [shown by a thick dotted line in Fig. 15(b)]. Figure 15 illustrates different evolutions of the capillary jet with $K=10^3$ at different values of the rescaled transfer coefficient $\bar{J}$ from 1 to 10^{-4}. Figure 15(a) shows the neck radius $R(0,t)$ versus time, and Fig. 15(b) shows the jet profiles at the end of each simulation.

The corresponding adsorbed surfactant concentrations are shown in Fig. 15(c) and the total surfactant coverage versus time is shown in Fig. 15(d).

In the limit of fast diffusion of bulk surfactant, surfactant is adsorbed onto the interface provided that the surface surfactant concentration is below the equilibrium value $\Gamma=\Gamma_{eq}=K/(K+1)$, and the data for Fig. 15 show that $\Gamma(z,t)<\Gamma_{eq}$ throughout these simulations in all cases. For the two largest values of the transfer coefficient shown, $\bar{J}=1$ and $\bar{J}=10^{-1}$, a significant amount of surfactant is adsorbed onto the interface at the beginning of the simulation. The jet is thus quickly covered with a nearly uniform surfactant concentration and the total surfactant coverage saturates, see Fig. 15(d). As a result, the jet contracts and pinches off much as a clean jet would, but more slowly since it has a reduced surface tension, and the jet profiles just before pinch-off [shown in Fig. 15(b)] are similar to those for a surfactant-free jet.

At smaller values of the transfer coefficient $\bar{J}\leq 10^{-2}$, reduced surfactant transport from the bulk allows the contraction to proceed in a similar way to the insoluble case up to $t\simeq 4$. The jet contracts due to capillary pressure in excess of internal pressure near $z=0$, and the local reduction in surface area leads to increased surfactant concentration and reduced surface tension and capillary pressure. If this process is fast compared to surfactant adsorption onto the interface, a quasisteady thread forms. Since $\Gamma<\Gamma_{eq}$ throughout the simulations, surfactant continues to be adsorbed onto the thread surface after the thread forms, and if pinch-off eventually takes place it occurs with a more elongated neck than in the surfactant-free case. This finding is consistent with the results of the direct numerical simulations in Sec. III A 1.

B. Numerical solution of the long-wave model: Large bulk Peclet number Pe=$O(1/\epsilon)$

In this subsection we present numerical results for the dynamics of a capillary jet with large bulk Peclet number. The same parameter values and initial profile for the adsorbed surfactant and jet shape in Sec. IV A are used. In this limit the surfactant exchange flux is computed from the radial gradient of the bulk surfactant concentration evaluated at the jet interface. The transfer coefficient J in Eq. (23) is varied in the range from 1 to 10^{-4} to show the effects of solubility. Figure 16(a) shows the neck radius $R(0,t)$ versus time, and Fig. 16(b) shows the jet profiles at the end of each simulation. The corresponding surfactant profiles are shown in Fig. 16(c) and the total surfactant coverage versus time is shown in Fig. 16(d).

Initially the bulk surfactant concentration in the neighborhood of the interface is

$$C_S(t=0^+)=\frac{\Gamma_i}{K(1-\Gamma_i)}\ll C_\infty=1,$$

with $\Gamma_i=0.4$ and $K=10^3$, and since the bulk Peclet number is large the normal gradient $|\boldsymbol{n}\cdot\nabla C|_S$ is large like Pe, per Eqs. (18) and (21). As a result, the initial surfactant exchange flux can be significant, with surfactant being adsorbed rapidly onto the interface unless the transfer coefficient J is small. For example, when $J=1$ the jet is almost uniformly covered

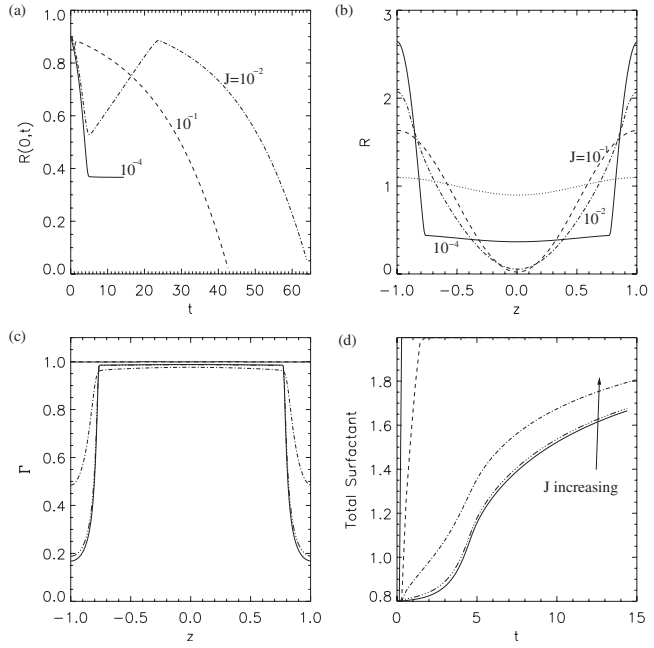

FIG. 16. Solution of the long-wave model in the limit of large bulk Peclet number Pe, with $K=10^3$ and $\mathrm{Pe}_s=\infty$, at different values of J: $J=1$ (thin solid line), $J=10^{-1}$ (dashed line), $J=10^{-2}$ (dot-dashed line), $J=10^{-3}$ (dot-dot-dot-dashed line), and $J=10^{-4}$ (thick solid line). (a) Neck radius $R(0,t)$ vs time t. (b) Profiles $r=R(z,t)$ at the end of each simulation. (c) The corresponding surfactant concentration profiles $\Gamma(z,t)$. (d) The total surfactant coverage vs time.

with a very high surfactant concentration shortly after $t=0$. The surface tension then reaches its minimal saturated value [$\sigma_{\min}=0.1$ of Eq. (10)] for the remainder of the simulation, and the jet pinches off under capillary pressure in much the same way as a clean jet but with reduced surface tension.

For $J\lesssim 10^{-1}$ the rate of adsorption of surfactant from the bulk is not as fast relative to the initial rate of contraction due to capillary instability, thereby postponing reduction in the surface tension to its minimum saturated value. The jet contracts at a faster rate at the beginning of the simulation compared to the case when $J=1$. However, for values of $J\lesssim 10^{-1}$ to $J\simeq 10^{-3}$ this initial contraction is followed by a period of restoring motion during which the thread returns toward its cylindrical shape. This occurs because reduction in the capillary pressure is sufficiently enhanced by surfactant adsorption from the bulk that the capillary pressure falls below the internal pressure before the minimum surface tension is reached. During the restoring process more surfactant is adsorbed onto the interface from the bulk, until the surface tension finally approaches its minimum saturated value. At this point, since the thread still has a minimum radius at $z=0$, a second phase of contraction begins with nearly uniform surface tension.

This is seen in Fig. 16(a) for the evolution of the neck radius $r=R(0,t)$ with $J=10^{-2}$. The jet initially contracts much as though the surfactant was insoluble, and a thread begins to form at $t\simeq 5$. Surfactant adsorption from the bulk then leads to restoring motion until the surface tension reaches its minimum saturated value at $t\simeq 25$. After $t\simeq 25$ the jet undergoes slow, nearly uniform surface tension con-

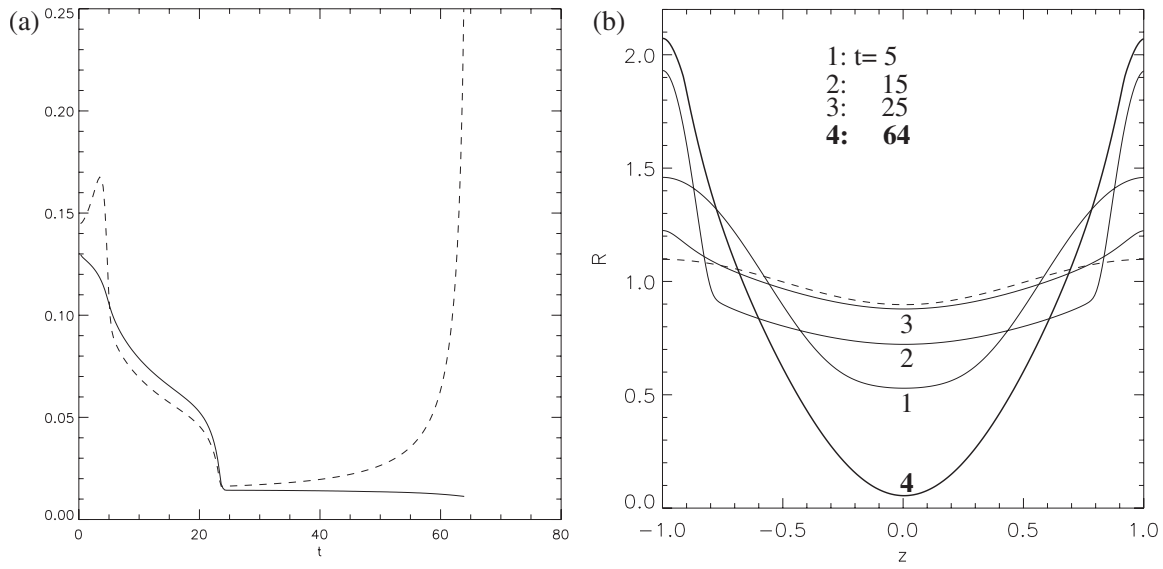

FIG. 17. Detail of the evolution in Fig. 16 when $J=10^{-2}$. (a) Internal pressure (solid line) and capillary pressure (dashed line) vs time. (b) Profiles $r=R(z,t)$ at times shown.

traction that eventually leads to pinch-off at $t\simeq 65$. More details are shown in Fig. 17, which shows the fall in capillary pressure to values below the internal pressure for $5\lesssim t\lesssim 25$ and the profiles $r=R(z,t)$ at a sequence of times.

We showed earlier[32] that for insoluble surfactant, the development of thread end constrictions, which is seen in the direct numerical simulations of Sec. III [see, e.g., Figs. 2(a), 6(b), and 9(c)], is caused by a small flux of surfactant leaving the thread ends and entering the parent bubble surface, and mechanisms that can cause this to occur include axial flow velocity, Marangoni stress, or surface diffusion of surfactant. In the direct numerical simulations, axial flow, and Marangoni stress are present and contribute to the flux but surface diffusion is absent since the surface Peclet number, which is typically large, has been set to $\mathrm{Pe}_s=\infty$. In the long-wave model, axial flow and Marangoni stress are excluded as higher order effects, per the discussion above Eq. (15). In our earlier work (Ref. 32 Sec. 5.1.1) studies of the long-wave model with the rescaled surface Peclet number $\overline{\mathrm{Pe}}_s$ both finite and infinite showed that the flux of an insoluble surfactant caused by surface diffusion introduces thread end constrictions in a way that closely mimics the influence of axial flow and Marangoni stress in the direct numerical simulations. It would appear that surfactant solubility is an additional mechanism that can cause or at least contribute to the same effect, with desorption from the region of high surface concentration occurring near the thread end, followed by advection and diffusion in the bulk flow and adsorption onto the parent bubble, as indicated by the rapid change in sign of the normal gradient $\boldsymbol{n}\cdot\nabla C|_S$ seen in Fig. 3. In the long-wave simulations of this study, we have set $\mathrm{Pe}_s=\infty$ to isolate solubility as the only mechanism available to cause constrictions to develop. However, since the data of Figs. 15(b) and 16(b) do not show constrictions forming, the effect appears to be small.

V. SUMMARY

We have investigated the influence of surfactant solubility on the evolution of a stretched inviscid bubble in a quiescent viscous flow by numerical solution of the Navier–Stokes equations. The bubble profile relaxes under the influence of surfactant-modified surface tension, and three parameters express the effects of surfactant solubility in the diffusion controlled regime. These are the transfer coefficient J, the partition coefficient for the relative rate of adsorption to desorption K, and the bulk Peclet number Pe.

In the limit of small J the influence of surfactant solubility is small, and the evolution is close to that with insoluble surfactant, as described earlier.[32] The initially dumbbell shaped bubble contracts at its narrowest point $z=0$ via capillary instability, with a velocity profile in the outer fluid that is nearly radial. The increase in surface concentration of surfactant due to contraction causes the capillary pressure to reduce until it approaches the internal pressure, further contraction then stops, and this process repeats in a wavelike fashion that propagates out from $z=0$ until a slender quasi-steady thread is formed that connects parent bubbles. An increase in J with other parameters fixed enables surfactant to desorb from the thread interface where its concentration is greatest, and lessens the reduction in capillary pressure. The bubble then proceeds toward pinch-off at $z=0$, but at a rate that is slower than in the surfactant-free case and with a more elongated neck near its minimum radius.

The evolution also follows that found with insoluble surfactant at sufficiently large values of the partition coefficient K, while at smaller K the rate of desorption relative to adsorption is sufficiently large that surfactant enters the bulk flow adjacent to the thread, where it can diffuse away from the interface, promoting elongated neck pinch-off near $z=0$.

An increase in bulk Peclet number Pe with other parameters fixed causes the width of a transition layer of bulk

surfactant that forms adjacent to the interface to decrease, enhancing surfactant exchange between the interface and bulk by increasing the magnitude of the normal derivative $\boldsymbol{n}\cdot\nabla C$ at the interface. Provided that J is not too large and K is not too small, a thread can form at all values of bulk Peclet number of the simulations (i.e., Pe from 1 to 10^3), but its radius steadily decreases due to surfactant desorption from the interface, and this occurs at a rate that is greater at large Pe.

This study has focused on the influence of surfactant solubility on the formation of a thread. We have not carried out a detailed study of the precise location and structure at pinch-off, and the results of the numerical simulations reported are estimated to lose accuracy for values of the radius $r=R(z,t)$ less than about 10^{-3}. However, we conclude that in general, when effects of solubility are small a thread can be established for some time, it develops constrictions at its ends, and the profile may ultimately be driven to pinch-off there. When effects of solubility are greater, pinch-off occurs earlier and is more likely to occur at the location of minimum initial radius. We also note that if the surface tension reaches its minimum saturated value at any point before contraction has ceased, further decrease in capillary pressure is stopped, with the result that pinch-off occurs nearby.

We have also developed long-wave asymptotic models for the influence of surfactant solubility on a capillary jet, in the two contrasting limits where bulk diffusion of surfactant is either fast (small Pe) or slow (large Pe). The models are closed at leading order, and as explained above Eq. (15), they therefore exclude the influence of the Marangoni stress and axial velocity, although surface diffusion of surfactant can be included by rescaling the surface Peclet number Pe_s. Close similarity is found between the evolution and the influence of parameters on the dynamics for the bubble and capillary jet. There is one notable difference, however. The large Peclet number model for a capillary jet predicts that for some parameter values (e.g., $J=10^{-2}$ of Figs. 16 and 17) the profile radius increases temporarily, between an initial and final phase of contraction. Since there is a rational interpretation for this type of evolution in terms of a separation of time scales for the effects of capillary instability and surfactant solubility, the behavior appears not to be an artifact of the long-wave model and has not yet been found by direct numerical simulation as a consequence of the computational cost and loss of accuracy of the numerical method at values of the bulk Peclet number above $\mathrm{Pe}=10^3$.

ACKNOWLEDGMENTS

This work was supported by the NSF under Grant Nos. DMS-0708977 and DMS-0354560. The simulations were conducted on the NJIT computing cluster, supported by the NSF/MRI under Grant No. DMS-0420590.

[1] S. L. Anna, N. Bontoux, and H. A. Stone, "Formation of dispersions using 'flow focusing' in microchannels," Appl. Phys. Lett. **82**, 364 (2003).
[2] O. Ozen, N. Aubry, D. T. Papageorgiou, and P. G. Petropolous, "Monodisperse drop formation in square microchannels," Phys. Rev. Lett. **96**, 144501 (2006).
[3] T. Thorsen, R. Roberts, F. Arnold, and S. Quake, "Coherent pattern formation in a non-equilibrium microfluidic device," Phys. Rev. Lett. **86**, 4163 (2001).
[4] O. A. Basaran, "Small-scale free surface flows with breakup: Drop formation and emerging applications," AIChE J. **48**, 1842 (2002).
[5] J. Eggers, "Nonlinear dynamics and breakup of free-surface flows," Rev. Mod. Phys. **69**, 865 (1997).
[6] D. Quere, "Fluid coating on a fiber," Annu. Rev. Fluid Mech. **31**, 347 (1999).
[7] H. A. Stone, "Dynamics of drop deformation and breakup in viscous fluids," Annu. Rev. Fluid Mech. **26**, 65 (1994).
[8] Lord Rayleigh, "On the instability of jets," Proc. London Math. Soc. **s1-10**, 4 (1878).
[9] Lord Rayleigh, "On the stability of a cylinder of viscous liquid under capillary force," Philos. Mag. **34**, 145 (1892).
[10] S. Tomotika, "On the instability of a cylindrical thread of a viscous liquid surrounded by another viscous fluid," Proc. R. Soc. London, Ser. A **150**, 322 (1935).
[11] M. P. Brenner, J. R. Lister, and H. A. Stone, "Pinching threads, singularities and the number 0.0304…," Phys. Fluids **8**, 2827 (1996).
[12] J. Eggers and T. F. Dupont, "Drop formation in a one-dimensional approximation of the Navier-Stokes equation," J. Fluid Mech. **262**, 205 (1994).
[13] D. T. Papageorgiou, "On the breakup of viscous liquid threads," Phys. Fluids **7**, 1529 (1995).
[14] P. Doshi, I. Cohen, W. W. Zhang, M. Siegel, P. Howell, O. A. Basaran, and S. R. Nagel, "Persistence of memory in drop breakup: The breakdown of universality," Science **302**, 1185 (2003).
[15] J. Eggers, "Theory of drop formation," Phys. Fluids **7**, 941 (1995).
[16] J. R. Lister and H. Stone, "Capillary breakup of a viscous thread surrounded by another viscous fluid," Phys. Fluids **10**, 2758 (1998).
[17] A. Sierou and J. R. Lister, "Self-similar solutions for viscous capillary pinch-off," J. Fluid Mech. **497**, 381 (2003).
[18] R. Suryo, P. Doshi, and O. A. Basaran, "Non-self-similar, linear dynamics during pinch-off of a hollow annular jet," Phys. Fluids **16**, 4177 (2004).
[19] W. W. Zhang and J. R. Lister, "Similarity solutions for capillary pinch-off in fluids of differing viscosity," Phys. Rev. Lett. **83**, 1151 (1999).
[20] G. I. Taylor, "The formation of emulsions in definable fields of flow," Proc. R. Soc. London, Ser. A **146**, 501 (1934).
[21] M. R. Booty and M. Siegel, "Steady deformation and tip-streaming of a slender bubble with surfactant in extensional flow," J. Fluid Mech. **544**, 243 (2005).
[22] R. A. DeBruijn, "Tipstreaming of drops in simple shear flows," Chem. Eng. Sci. **48**, 277 (1993).
[23] C. D. Eggleton, T.-M. Tsai, and K. J. Stebe, "Tip streaming from a drop in the presence of surfactants," Phys. Rev. Lett. **87**, 048302 (2001).
[24] S. L. Anna and H. C. Mayer, "Microscale tipstreaming in a microfluidic flow focusing device," Phys. Fluids **18**, 121512 (2006).
[25] P. T. McGough and O. A. Basaran, "Repeated formation of fluid threads in breakup of a surfactant-covered jet," Phys. Rev. Lett. **96**, 054502 (2006).
[26] S. Hansen, G. W. M. Peters, and H. E. H. Meijer, "The effect of surfactant on the stability of a fluid filament embedded in a viscous fluid," J. Fluid Mech. **382**, 331 (1999).
[27] M.-L. E. Timmermans and J. R. Lister, "The effect of surfactant on the stability of a liquid thread," J. Fluid Mech. **459**, 289 (2002).
[28] S. Whitaker, "Studies of the drop-weight method for surfactant solutions: III. Drop stability, the effect of surfactants on the stability of a column of liquid," J. Colloid Interface Sci. **54**, 231 (1976).
[29] B. Ambravaneswaran and O. A. Basaran, "Effects of insoluble surfactants on the nonlinear deformation and breakup of stretching liquid bridges," Phys. Fluids **11**, 997 (1999).
[30] S. Kwak and C. Pozrikidis, "Effect of surfactants on the instability of a liquid thread or annular layer. Part I. Quiescent fluids," Int. J. Multiphase Flow **27**, 1 (2001).
[31] Y.-C. Liao, E. I. Franses, and O. A. Basaran, "Deformation and breakup of a stretching liquid bridge covered with an insoluble surfactant monolayer," Phys. Fluids **18**, 022101 (2006).
[32] M. Hameed, M. Siegel, Y.-N. Young, J. Li, M. R. Booty, and D. T. Papageorgiou, "Influence of insoluble surfactant on the deformation and breakup of a bubble or thread in a viscous fluid," J. Fluid Mech. **594**, 307 (2008).
[33] G. I. Taylor, *Proceedings of the 11th International Congress of Theoretical Applied Mechanics*, Munich, 1964 (Springer Verlag, Heidelberg, 1964), pp. 790–796.
[34] S. S. Sadhal and R. E. Johnson, "Stokes flow past bubbles and drops

partially coated with thin films. Part 1. Stagnant cap of surfactant: Exact solution," J. Fluid Mech. **126**, 237 (1983).
[35]C. M. Z. He and Z. Dagan, "The size of stagnant caps of bulk soluble surfactants on interfaces of translating fluid droplets," J. Colloid Interface Sci. **146**, 442 (1991).
[36]Y. Liao and J. B. McLaughlin, "Bubble motion in aqueous surfactant solutions," J. Colloid Interface Sci. **224**, 297 (2000).
[37]Y. Liao, J. Wang, R. J. Nunge, and J. B. McLaughlin, "Comment on 'Bubble motion in aqueous surfactant solutions'," J. Colloid Interface Sci. **272**, 498 (2004).
[38]R. Palaparthi, D. T. Papageorgiou, and C. Maldarelli, "Theory and experiments on the stagnant cap regime in the motion of spherical surfactant-laden bubbles," J. Fluid Mech. **559**, 1 (2006).
[39]Y. Wang, D. T. Papageorgiou, and C. Maldarelli, "Increased mobility of a surfactant retarded bubble at high bulk concentrations," J. Fluid Mech. **390**, 251 (1999).
[40]W. J. Milliken and L. G. Leal, "The influence of surfactant on the deformation and breakup of a viscous drop: The effect of surfactant solubility," J. Colloid Interface Sci. **166**, 275 (1994).
[41]R. A. Johnson and A. Borhan, "Stability of the shape of a surfactant-laden drop translating at low Reynolds number," Phys. Fluids **12**, 773 (2000).
[42]M. Muradoglu and G. Tryggvason, "A front-tracking method for computation of interfacial flows with soluble surfactants," J. Comput. Phys. **227**, 2238 (2008).
[43]J. Zhang, D. M. Eckmann, and P. S. Ayyaswamy, "A front tracking method for a deformable intravascular bubble in a tube with soluble surfactant," J. Comput. Phys. **214**, 366 (2006).
[44]R. G. M. van der Sman and S. van der Graaf, "Diffuse interface model of surfactant adsorption onto flat and droplet interfaces," Rheol. Acta **46**, 3 (2006).
[45]F. Jin, N. R. Gupta, and K. J. Stebe, "The detachment of a viscous drop in a viscous solution in the presence of a soluble surfactant," Phys. Fluids **18**, 022103 (2006).
[46]C. H. Chang and E. Franses, "Adsorption dynamics of surfactants at the air/water interface: A critical review of mathematical models, data, and mechanisms," Colloids Surf., A **100**, 1 (1995).
[47]J. Donea and A. Huerta, *Finite Element Methods for Flow Problems* (Wiley, New York, 2003).
[48]P. K. Notz, A. U. Chen, and O. A. Basaran, "Satellite drops: Unexpected dynamics and change of scaling during pinch-off," Phys. Fluids **13**, 549 (2001).
[49]E. D. Wilkes, S. D. Phillips, and O. A. Basaran, "Computational and experimental analysis of dynamics of drop formation," Phys. Fluids **11**, 3577 (1999).
[50]J. Li, M. Hesse, J. Ziegler, and A. W. Woods, "An arbitrary Lagrangian Eulerian method for moving-boundary problems and its application to jumping over water," J. Comput. Phys. **208**, 289 (2005).
[51]J. Li, "The effect of an insoluble surfactant on the skin friction of a bubble," Eur. J. Mech. B/Fluid **25**, 59 (2006).